

Guided Noise Reduction with Streak Removal for High Speed Flat Detector CT Perfusion

Michael T. Manhart, André Aichert, Markus Kowarschik, Yu Deuerling-Zheng, Tobias Struffert, Arnd Doerfler, Andreas K. Maier and Joachim Hornegger

Abstract—Tissue perfusion measurement using C-arm angiography systems capable of CT-like imaging (flat detector CT (FD-CT)) is a novel technique with high potential benefit for catheter-guided treatment of stroke in the interventional suite. New high speed protocols (HSP) with increased C-arm rotation speed enable fast acquisitions of FD-CT volumes and allow for sampling the contrast flow with improved temporal resolution. However, the peak contrast attenuation values of brain tissue typically lie in a range of 5–30 HU. Thus perfusion imaging is very sensitive to noise. Recently we introduced the FDK-JBF denoising technique based on Feldkamp (FDK) reconstruction followed by denoising in volume space using joint bilateral filtering (JBF). In the evaluation FDK-JBF achieved comparable results to algebraic techniques, but is computationally less costly. Yet the angular sampling of the projection data in the HSP is coarse, which leads to streak artifacts in the reconstructed volumes. Mask volumes are subtracted from the contrast agent enhanced (bolus) volumes and the streak artifacts are subtracted out if the patient does not move during the acquisition. However, in case of motion the streak artifacts will not be identical in the mask and bolus volumes. We show that these streaks can lead to severe artifacts in the perfusion maps and describe a novel technique for streak removal (SR), which is based on streak detection by using time-contrast curve analysis. We evaluated the FDK-SR-JBF algorithm in a phantom and a patient study and show that noise and streaks can be reduced within a short computation time.

Index Terms—Perfusion imaging, noise reduction, Flat detector CT, stroke treatment

I. INTRODUCTION

Perfusion CT (CTP) is an important imaging modality for diagnosis of ischemic stroke. Time attenuation curves (TACs) in tissue and vessels are extracted from a time series of brain volumes acquired after a contrast bolus injection. Perfusion parameter maps calculated from TACs which represent quantities such as cerebral blood flow (CBF), cerebral blood volume (CBV), mean transit time (MTT), and time-to-peak (TTP) provide information about the extent of the affected tissue. They can be used to identify potentially salvageable ischemic tissue that may be re-perfused by stroke therapy procedures, e.g. catheter-guided intra-arterial thrombolysis [1]. For this purpose the patient is transported to an interventional suite equipped with a C-arm angiography system. If perfusion

imaging were available on interventional C-arm systems it would save the time of moving the patient from a CT scanner room and allow intraoperative imaging to determine treatment success and endpoint. Additionally, flat detector CT perfusion (FD-CTP) can – in contrast to CTP – acquire 3D perfusion maps in high resolution in z (axial) direction with full brain coverage.

However, FD-CTP is challenging: common C-arm systems typically need 5 s to acquire one volume, which limits the temporal resolution of the reconstructed TACs. Furthermore perfusion imaging is highly sensitive to noise since the peaks of the TACs inside the brain tissue typically lie in a range of 5–30 HU. Recently, novel techniques to overcome these challenges were proposed [2]. For instance, Wagner et al. [3] presented an algebraic algorithm modeling TACs as gamma-variate functions. We used a dynamic algebraic reconstruction technique [4] to reconstruct TACs with increased temporal resolution from the acquired X-ray projections and apply regularization based on joint bilateral filtering (JBF) [5] to increase the contrast-to-noise ratio (CNR) of the brain tissue TACs. However, the algebraic approaches have a much higher computational effort than Feldkamp (FDK) [6] reconstruction. A further possibility to improve the temporal sampling of the TACs is a high speed protocol with increased rotation speed of up to 100°/s using novel robotic C-arm systems (Artis zeego, Siemens AG, Germany). To deal with the low contrast signal in the brain tissue, we recently proposed a reconstruction scheme (FDK-JBF) based on FDK reconstruction followed by iterative denoising in volume space using JBF [7]. In a digital brain phantom study simulating the high speed protocol, the FDK-JBF technique produced brain perfusion maps with good correlation to ground truth maps and comparable quality as computationally more expensive algebraic reconstruction techniques. However, due to limitations in the detector read out rate, the angular sampling of the projection data in high speed scanning is coarse. This leads to streak artifacts in the reconstructed volumes. Since mask volumes are subtracted from the bolus volumes to compute the pure contrast agent enhancement, the streak artifacts are subtracted out. In practical applications the patient might move during the acquisition. The motion can be compensated by rigid registration, but the streak artifacts will not be identical in the mask and bolus volumes anymore and visible in the pure contrast volumes. In this work, we show that these streaks can lead to severe artifacts in the perfusion maps and describe a novel technique for FD-CTP streak removal (SR), which is based streak detection using time curve analysis.

M. T. Manhart, A. Aichert, A. K. Maier and J. Hornegger are with Pattern Recognition Lab, Department of Computer Science, Friedrich-Alexander-Universität Erlangen-Nürnberg, Martensstr. 3, 91058 Erlangen, Germany. M. Kowarschik and Y. Deuerling-Zheng are with Siemens AG, Angiography & Interventional X-Ray Systems, Forchheim, Germany. A. Aichert, T. Struffert and A. Doerfler are with Departments of Neuroradiology, Universitätsklinikum Erlangen, Erlangen, Germany.

Email: michael.manhart@cs.fau.de

The high speed protocol consists of twelve alternating C-arm rotations: the first two rotations acquire mask volumes with static anatomical structures in forward and backward C-arm rotation before bolus injection. The following ten consecutive rotations after bolus injection acquire a time series of bolus volumes in alternating forward and backward C-arm rotation. Each rotation acquires 133 projections over a 200° angular range and requires $T_r = 2.8$ s for data acquisition with a pause of $T_w = 1.2$ s between any two successive rotations. Thus, TACs can be acquired with a temporal sampling of $T_s = T_r + T_w = 4$ s.

II. ALGORITHM

This work presents an extension to the FDK-JBF algorithm [7]. The novel FDK-SR-JBF algorithm as shown in Figure 1 constitutes a standard FDK reconstruction (Steps 1–3), the JBF denoising (Steps 4–7 and 13–16) and additionally the proposed streak artifact detection and removal (Steps 8–12). The parameters for the algorithms used in this work are shown in Table I. The single steps and the algorithm parameters are discussed in detail in this section.

In Step 1 all mask and bolus acquisitions are reconstructed using the FDK algorithm. A non-smoothing Shepp-Logan filter kernel [8] is used to preserve the edges around the high contrast vessels. To compensate for head motion during the acquisition, all reconstructed volumes are registered to the forward mask volume in step 2 using 3D-3D rigid registration [9]. In Step 3 the reconstructed mask volumes are subtracted from the bolus volumes to obtain the contrast volumes describing the pure contrast agent enhancement over time.

In Steps 4 the guidance volume M is computed by finding the peak contrast attenuation over all contrast volumes for each voxel. The guidance image M is denoised by bilateral filtering [10], [11] with range variance σ_{R0}^2 and domain variance σ_D^2 in Step 5. An example for M is shown in Figure 3a. In Step 6 the contrast volumes are denoised by joint bilateral filtering of each volume with range variance σ_R^2 and domain variance σ_D^2 . The JBF corresponds to bilateral filtering, where the range similarity is computed using the guidance volume M . In Step 7 M is updated by recomputing the peaks from the filtered contrast enhanced volumes. This first JBF before the streak removal is required to generate data with sufficient contrast-to-noise ration (CNR) for the TAC analysis in Step 9.

In addition to high contrast vessels, M can contain edges due to streak artifacts (Figure 3a). If we do not detect and remove these false edges, they will be translated to the filtered contrast volumes. We suggest to identify voxels that are affected by streaks based on their intensity and TACs. Therefore, we identify the brain tissue in Step 8 by segmenting the forward mask volume in to air, bone and tissue by thresholding. Voxels with a radiodensity below τ_{Air} are classified as air, voxels with a radiodensity above τ_{Bone} are classified as bone and the remaining voxels are classified as brain tissue. In Step 9 streaks and vessels are identified by thresholding M followed by time curve analysis. If a tissue voxel in M is below $\tau_{M_min} \leq 0$, it is classified as streak. No negative radiodensity values are expected in the contrast attenuation peaks, except slightly

negative values due to noise or registration errors. If the a tissue voxel in M has a large intensity above $\tau_{M_max} > 0$, it can be either a vessel or a streak. To differentiate between vessels and streaks, the TACs are analyzed. Vessels have typical TACs with monotonic increase up to a clear contrast peak and possibly a second smaller peak due to second pass, while streaks tend to produce irregular TACs. Figure 2 shows a typical arterial TAC compared to a TAC observed at a streak. We denote the difference of the peak value to the value from which the monotonic increase to the peak starts as the uptake μ . Figure 2 shows the uptake of the dominant peak of an arterial TAC. To differentiate streaks and vessels, a voxel is identified as vessel if its corresponding TAC has:

- 1) a single global peak with an uptake μ_{global} of at least $\nu_{global} = 70\%$ of the peak value itself,
- 2) no further peak with an uptake μ_{local} of more than $\nu_{local} = 30\%$ of the global peak uptake μ_{global} .

Otherwise, this voxel is classified as streak. Step 10 classifies tissue voxels of all other intensities as streaks if they have a total variation (TV) above τ_{TV} . Figure 3c shows the TV image of M . The final brain segmentation is generated in Step 11 by combining the detected streaks and vessels. First a dilation operation on segmented vessels using a 2D rectangular element of size 2×2 voxels is applied. The dilation of the vessels ensures that the vessel edges are preserved in the streak removal step. Then an erosion (1×2 element) followed by dilation (2×2 element) operation is applied to the streak mask to remove single outliers and close gaps in the detected streak areas. Finally the brain segmentation is created by combining the vessel and streak masks with the initial brain tissue segmentation. If after dilation one voxel is identified as streak and vessel, it is classified as vessel. An example segmentation result is shown in Figure 3d. In Step 12, the identified streaks are removed by smoothing with a truncated Gaussian kernel averaging over spatial close tissue voxels which are not classified as vessels. Figure 3b shows M after the streak reduction was applied. Finally, $N_{it} = 3$ JBF denoising iterations are applied on the original reconstructed data in Steps 13–16 using the streak reduced MIP M as guidance image for noise reduction and streak removal in the perfusion data.

After reconstruction TACs sampled in 1 s intervals are generated from the reconstructed volumes by linear interpolation and an appropriate arterial input function (AIF) is selected manually. In case of pure FDK reconstruction the data is denoised after AIF selection by filtering spatially using a 2D Gaussian kernel with domain variance σ_C^2 . Then CBF and CBV maps are computed using a deconvolution-based approach [12].

III. MATERIALS & METHODS

A. Brain Phantom Simulation Study

To evaluate the streak reduction technique in a simulation study we use a digital brain perfusion phantom [13], [4]. The digital brain phantom is based on MR data and does not have the sparse structures of classical CT phantoms, which favor algorithms applying typical non-linear filters. Furthermore, we

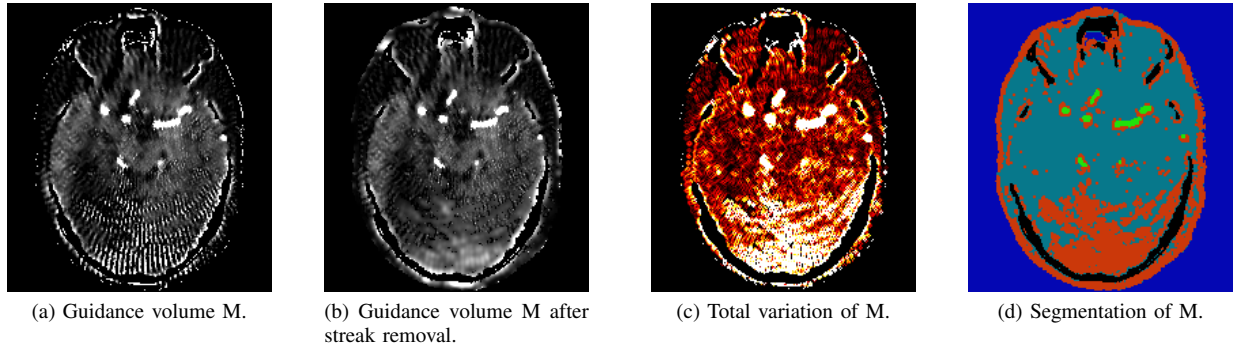


Figure 3: Slice from guidance volume M before and after streak removal, total variation and segmentation slice from original guidance image. Segmentation legend: orange: streaks, light green: vessels, dark green: tissue, black: bone, blue: air.

- 1) FDK reconstruction of mask & bolus acquisitions
- 2) Motion compensation by rigid 3D-3D registration
- 3) Compute pure contrast volumes by mask subtraction
- 4) Compute temporal maximum intensity projection M
- 5) Bilateral filtering of M
- 6) Joint bilateral filtering of pure contrast volumes
- 7) Recompute M from filtered volumes
- 8) Segment brain tissue by thresholding mask volume
- 9) Identify vessels and streaks by thresholding M and time curve analysis
- 10) Identify streaks by thresholding of TV (M)
- 11) Create final brain segmentation
- 12) Remove streaks in M by smoothing
- 13) For $k = 1 \dots N_{it}$
- 14) Joint bilateral filtering of pure contrast volumes
- 15) Recompute M from filtered volumes
- 16) End For

Figure 1: FDK-SR-JBF algorithm.

Parameter	Value	Parameter	Value
JBF kernel size	$7 \times 7 \times 7$ voxel	τ_{M_min}	$-5 \Delta HU$
σ_D	1.5 voxel	τ_{M_max}	150 ΔHU
σ_R	10 HU (simulations) 20 HU (clinical data)	τ_{TV}	20 ΔHU
σ_{R0}	120 HU	ν_{global}	70 %
τ_{Air}	- 800 HU	ν_{local}	30 %
τ_{Bone}	350	σ_G	2 voxel
N_{it}	3		

Table I: FDK-SR-JBF algorithm parameters.

incorporate the cortical bone structures of a human skull for a realistic simulation of streak artifacts. The skull was generated from a dedicated MR scan sequence of a human brain using the MR skull segmentation algorithm by Navalpakkam et al. [14]. Patient motion was simulated by rotation of the bolus volumes by 2° relative to the mask volume around the z axis before generating the projection data. Ellipsoid ROIs simulating tissue with reduced and severely reduced perfusion were annotated in the brain phantom. We created dynamic C-arm projection data by forward projection the 4D brain phantom according to the high speed protocol. Afterward Poisson distributed noise was added to the projection data

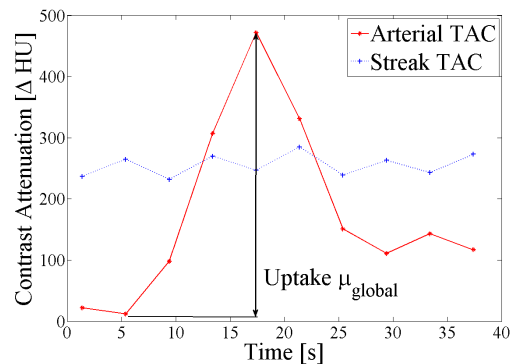


Figure 2: Time-contrast attenuation curves in an artery and in streak-affected brain tissue.

simulating an emitted X-ray density of $6 \cdot 10^5$ photons per mm^2 at the detector and a monochromatic photon energy of 60 keV. The combination of the complex brain structure, the high contrast skull and the patient movement simulation allows a realistic numerical evaluation of the denoising and streak removal algorithms.

For quantitative evaluation of the reconstructed perfusion maps we calculated the Pearson correlation (PC) between the reconstructed and the ground truth maps by applying an automated ROI analysis. The slices of the perfusion maps with stroke annotation were partitioned into quadratic areas of 4×4 pixels. The average perfusion values of the ROIs were calculated and used as measurement variables for the PC computation. ROIs containing vascular structures, bone, or air were ignored.

B. Clinical Patient Data

Real clinical patient data acquired with the high speed scanning protocol during an interventional stroke treatment was used for evaluation. Since the patient moved slightly between mask and contrast acquisitions, severe streak artifacts arise in the perfusion maps created with the original FDK-JBF algorithm. We also reconstructed the data with a total variation based algebraic reconstruction approach with ordered subsets (OS-TV). The OS-TV uses the algebraic reconstruction

framework from [7] and TV regularization with automatic adaption of the TV gradient step size as proposed in the iTV algorithm [15]. The algebraic OS-TV reconstruction technique helped to remove the streaks without blurring the edges at the high contrasted vessels for the price of a higher computational complexity. We also applied the FDK-SR-JBF for denoising and streak removal and compare the reconstructed CBF maps qualitatively to the OS-TV, FDK-JBF, and FDK results.

IV. RESULTS

Figure 4 shows the resulting CBF maps reconstructed from the brain phantom projection data with different approaches compared to the reference. The quantitative results of the brain perfusion study are shown in Table II. Figure 5 shows CBF maps from a clinical patient study comparing FDK-JBF, FDK-SR-JBF, and OS-TV reconstruction results and the corresponding computation time. The volumes had a size of $256 \times 256 \times 180$ voxels and were reconstructed on a workstation with 8 Intel(R) Xeon(R) W3565 CPUs with 3.20 GHz, 12 GB RAM, and an NVIDIA(R) Quadro FX 5800 display adapter.

V. DISCUSSION

The perfusion maps in the upper row of Figure 4 show that the CBF maps created by using FDK-JBF and FDK-SR-JBF approaches are less noisy and the stroke affected areas are much better separated from the healthy tissue than in the FDK approach. However, the FDK-JBF map in the lower row of Figure 4 shows how the non-linear denoising also preserves or even enhances streaks. Using the FDK-SR-JBF approach, these streaks can be successfully removed. The CBF maps created from the real clinical patient data shown in Figure 5 confirm the results of the simulation study: the FDK-JBF provides less noisy results than the FDK method, but shows severe streak artifacts in the lower part of the brain. The FDK-SR-JBF and OS-TV methods allow edge preserving denoising in combination with streak removal. The FDK-SR-JBF method produces very similar CBF maps as the OS-TV algorithm. However, the computation time of OS-TV was with ~ 25 min by a factor of more than ~ 25 higher than the computation time of FDK-SR-JBF with ~ 1 min.

VI. CONCLUSIONS

In this work we presented a novel method for computational fast noise reduction and streak removal in flat detector CT perfusion data acquired with a high speed scanning protocol. We expose that our previously published FDK-JBF [4] denoising technique can produce perfusion maps heavily corrupted by streak artifacts in case of coarse angular projection sampling and patient motion. Hence we extend the FDK-JBF technique by including a streak removal (SR) method to the FDK-SR-JBF algorithm. Therefore the brain is segmented into tissue, vessels and streaks using information from temporal maximum intensity projection, the contrast-time attenuation curves and total variation calculation. Subsequently the streaks are removed by smoothing the identified areas in the JBF guidance image. Our evaluation using digital brain perfusion phantom and real clinical patient data shows the potential of

the FDK-SR-JBF approach for robust denoising and streak removal in flat detector CT perfusion.

Disclaimer: The concepts and information presented in this paper are based on research and are not commercially available. The patient study has been approved by the ethics commission of the Medical Faculty at Friedrich-Alexander-Universität Erlangen-Nürnberg, Germany, Ethik-No. 4535 on Dec 14th 2011.

REFERENCES

- [1] A. Furlan, R. Higashida, L. Wechsler, M. Gent, H. Rowley, C. Kase, M. Pessin, A. Ahuja, F. Callahan, W. M. Clark, F. Silver, and F. Rivera, "Intra-arterial prourokinase for acute ischemic stroke: The PROACT II study: A randomized controlled trial," *JAMA*, vol. 282, pp. 2003–2011, 1999.
- [2] A. Fieselmann and M. T. Manhart, "Interventional perfusion imaging using C-Arm CT," *Current Medical Imaging Reviews*, vol. 9, no. 2, pp. 96–101, 2013.
- [3] M. Wagner, Y. Deuerling-Zheng, M. Möhlenbruch, M. Bendszus, J. Boese, and S. Heiland, "A model based algorithm for perfusion estimation in interventional C-arm CT systems," *Medical Physics*, vol. 40, no. 3, pp. 0319161–03191611, 2013.
- [4] M. T. Manhart, M. Kowarschik, A. Fieselmann, Y. Deuerling-Zheng, K. Royalty, A. K. Maier, and J. Hornegger, "Dynamic iterative reconstruction for interventional 4-D C-arm CT perfusion imaging," *Medical Imaging, IEEE Transactions on*, vol. 32, no. 7, pp. 1336–1348, July 2013.
- [5] G. Petschnigg, M. Agrawala, H. Hoppe, R. Szeliski, M. Cohen, and K. Toyama, "Digital photography with flash and no-flash image pairs," in *Proc. ACM SIGGRAPH*, vol. 23, no. 3, 2004, pp. 664–672.
- [6] L. Feldkamp, L. Davis, and J. Kress, "Practical cone-beam algorithm," *Journal of the Optical Society of America A*, vol. 1, no. 6, pp. 612–619, 1984.
- [7] M. T. Manhart, A. Fieselmann, Y. Deuerling-Zheng, and M. Kowarschik, "Iterative denoising algorithms for perfusion C-arm CT with a rapid scanning protocol," in *Proc. IEEE ISBI*, 2013, pp. 1223–1227.
- [8] L. Shepp and B. Logan, "The Fourier reconstruction of a head section," *IEEE Trans Nuclear Science*, vol. 21, pp. 21–43, 1974.
- [9] P. Viola and W. M. Wells III, "Alignment by maximization of mutual information," *International Journal of Computer Vision*, vol. 24, no. 2, pp. 137–154, 1997.
- [10] V. Aurich and J. Weule, "Non-linear Gaussian filters performing edge preserving diffusion," *Proc. DAGM-Symposium Mustererkennung*, vol. 17, pp. 538–545, 1995.
- [11] C. Tomasi and R. Manduchi, "Bilateral filtering for gray and color images," in *Proc. 6th IEEE ICCV*, 1998, pp. 839–846.
- [12] A. Fieselmann, M. Kowarschik, A. Ganguly, J. Hornegger, and R. Fahrig, "Deconvolution-based CT and MR brain perfusion measurement: Theoretical model revisited and practical implementation details," *International Journal of Biomedical Imaging*, 2011, article ID 467563.
- [13] A. J. Riordan, M. Prokop, M. A. Viergever, J. W. Dankbaar, E. J. Smit, and H. W. A. M. de Jong, "Validation of CT brain perfusion methods using a realistic dynamic head phantom," *Medical Physics*, vol. 38, no. 6, pp. 3212–3221, 2011.
- [14] B. K. Navalpakkam, H. Braun, T. Kuwert, and H. H. Quick, "Magnetic Resonance-Based Attenuation Correction for PET/MR Hybrid Imaging Using Continuous Valued Attenuation Maps," *Invest Radiol*, vol. 48, no. 5, pp. 323–332, May 2013.
- [15] L. Ritschl, F. Bergner, C. Fleischmann, and M. Kachelrieß, "Improved total variation-based CT image reconstruction applied to clinical data," *Physics in Medicine and Biology*, vol. 56, no. 6, pp. 1545–1561, 2011.

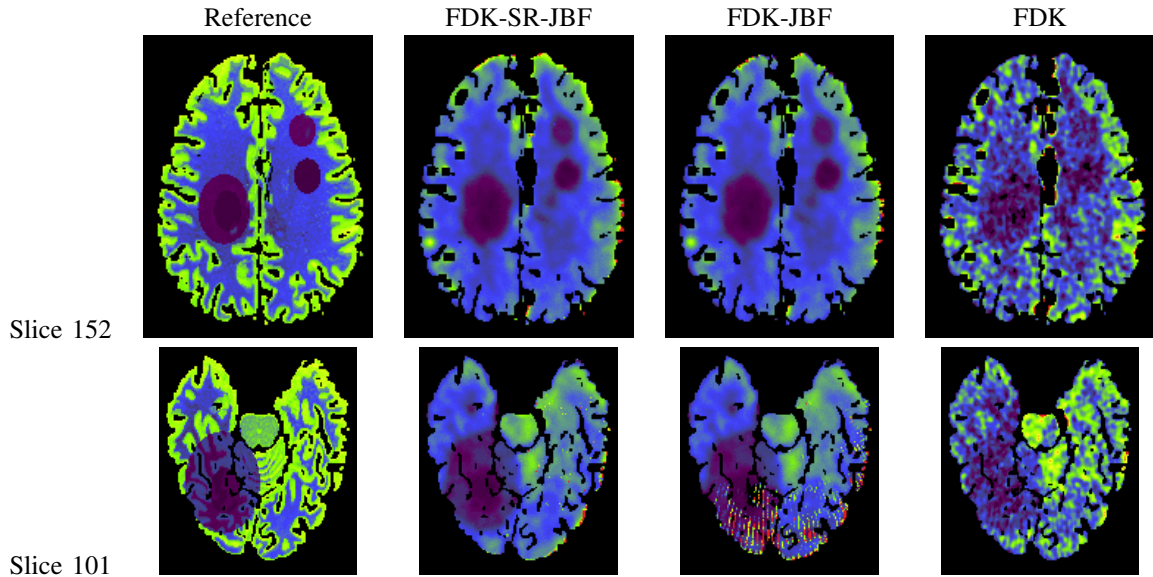


Figure 4: Two slices of brain phantom CBF maps reconstructed with different approaches.

	FDK	FDK-JBF	FDK-SR-JBF
Pearson Correlation CBF	0.76	0.80	0.83
Pearson Correlation CBV	0.63	0.68	0.73

Table II: Quantitative results of brain phantom study. Pearson correlation of CBF and CBV perfusion maps reconstructed with different approaches to the ground truth maps.

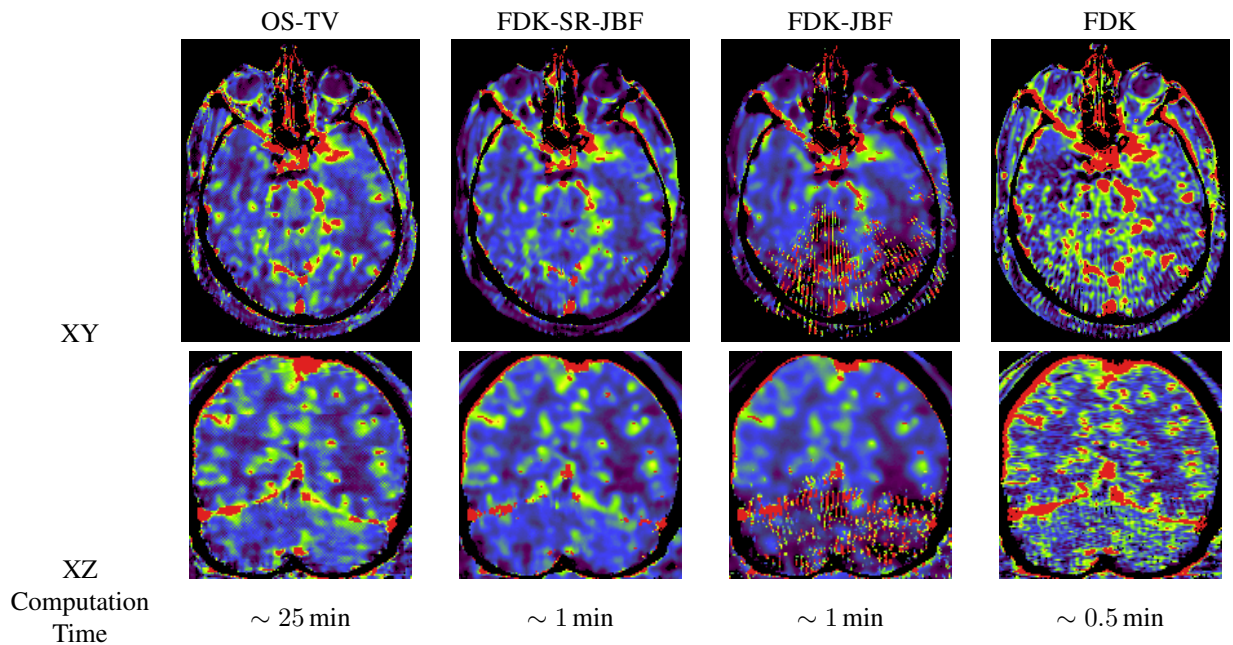


Figure 5: Patient CBF maps in XY and XZ viewing direction reconstructed with different algorithms.